University of Sistan and Baluchestan

Chemical Process Design

Available online at http://cpd.usb.ac.ir/

Uncertainty-Quantified Kinetic Model Discrimination for Photocatalytic Reactor Design: A Bootstrap Based Framework

Masoud Khajenoori[1]✉

[1] Catalytic Process Design and Simulation Laboratory, Department of Chemical Engineering, Faculty of Engineering, University of Kashan, Kashan, Iran. Email: khajenoori@kashanu.ac.ir

ARTICLE INFO

Article type:
Research Article

Article history:
Received: 2026-05-16
Received in revised form: 2026-07-04
Accepted: 2026-07-28
Available online: 2026-07-28

Keywords: *Photocatalytic reactor design; Kinetic model; Akaike Information Criterion; Uncertainty quantification; Bootstrap resampling; Optimization.*

ABSTRACT

Translating laboratory-scale photocatalytic batch data into continuous reactor design remains a critical challenge in reaction engineering, particularly when kinetic model selection is based solely on the coefficient of determination (R^2) and parameter uncertainty is ignored. In this study, a data-driven framework is developed that integrates nonlinear kinetic model discrimination, bootstrap-based uncertainty quantification, and uncertainty propagation into plug-flow reactor (PFR) sizing. Time–concentration data from methylene blue degradation over a $WO_3/BiVO_4$ photocatalyst (C_0 = 10mgL^{-1}) were fitted to six nonlinear kinetic models using Particle Swarm Optimization (PSO). Model discrimination was performed using the bias-corrected Akaike Information Criterion (AICc) and Akaike weights, decisively selecting the Elovich model (ΔAICc > 30 vs. pseudo-first-order; Akaike weight > 0.99). Parameter uncertainty was quantified via nonparametric bootstrap resampling (2000 replicates), yielding well-constrained 95% confidence intervals (α: 2.02-2.28mgg^{-1}min^{-1}; β: 0.34-0.42gmg^{-1}). The identified kinetics were embedded into a steady-state PFR model, and bootstrap parameter distributions were propagated to generate a reactor length design envelope for 90% pollutant removal. The nominal reactor length was 1.25m, with a 95% confidence interval of 1.18-1.35m (±7%). This narrow design envelope demonstrates robust parameter identifiability and provides a statistically defensible basis for reactor sizing, moving beyond single-point deterministic estimates. The proposed methodology offers a transferable framework for integrating nonlinear kinetic discrimination and uncertainty quantification into photocatalytic reactor engineering.

Cite this article: Khajenoori, M., (2026), Uncertainty-Quantified Kinetic Model Discrimination for Photocatalytic Reactor Design: A Bootstrap Based Framework, *Chemical Process Design*, 5(2), 89-102. http//doi.org/10.22111/cpd.2026.55388.1088

DOI: http//doi.org/10.22111/cpd.2026.55388.1088

Publisher: University of Sistan and Baluchestan.

1. Introduction

Heterogeneous photocatalysis has been extensively investigated as an advanced oxidation process for the degradation of recalcitrant organic pollutants in wastewater [1, 2]. Among emerging photocatalytic materials, visible-light-responsive semiconductors such as WO_3 and $BiVO_4$ have attracted considerable attention due to their favorable band-edge alignment, suitable band gaps, and potential operation under solar irradiation [3-5]. $WO_3/BiVO_4$ heterojunction systems, in particular, have been reported to enhance charge separation efficiency and suppress electron–hole recombination [6, 7]. Despite extensive material-level development, the translation of laboratory-scale photocatalytic performance into continuous-flow reactor design remains a persistent gap. Most published studies report degradation efficiencies under batch conditions without extracting transferable kinetic parameters suitable for engineering calculations [8-10]. Early reactor modeling efforts highlighted the importance of integrating kinetics with hydrodynamic and radiative effects, yet comprehensive data-driven scale-up methodologies remain scarce [11]. A critical methodological weakness in many photocatalytic kinetic studies is the reliance on linearized pseudo-first-order expressions and the coefficient of determination (R^2) as the sole criterion for model selection. Linearization alters the statistical structure of experimental errors and may bias parameter estimation [12, 13]. Furthermore, R^2 is an inadequate measure for evaluating nonlinear regressions, as it monotonically increases with the number of parameters and cannot penalize model complexity [14]. Information-theoretic criteria, such as the Akaike Information Criterion (AIC), offer an objective basis for comparing competing nonlinear models while accounting for parsimony [15]. Despite their widespread use in ecological and biological modeling, AIC-based approaches remain underutilized in photocatalytic kinetic studies. An equally important but often neglected issue is the propagation of kinetic parameter uncertainty into reactor design. Parameter estimates obtained from limited batch data inherently possess uncertainty, yet conventional reactor sizing typically employs point estimates, yielding a single deterministic reactor length without any confidence bounds [16]. This practice obscures the reliability of the design and may lead to over or under sizing in practice. Structural and practical identifiability considerations play a critical role in determining whether estimated parameters can be reliably interpreted and propagated into reactor design calculations [17]. Bootstrap resampling provides a flexible, nonparametric approach for quantifying parameter uncertainty without requiring assumptions about the error distribution [18, 19].

The present study addresses these methodological gaps by asking the following research question: How can limited batch concentration time data be translated into statistically defensible reactor design envelopes for visible-light photocatalytic systems? To answer this question, we develop an integrated data-driven framework that:

(*i*) performs nonlinear kinetic model discrimination among six competing formulations pseudo-first-order (PFO) [11], pseudo-second-order (PSO) [20], Elovich [21], Avrami [22], intraparticle diffusion (IPD) [23], and modified Langmuir Hinshelwood (MLH) [24] using the bias-corrected Akaike Information Criterion (AICc) and Akaike weights [15];

(*ii*) estimates kinetic parameters via Particle Swarm Optimization (PSO) [25] and quantifies their uncertainty through nonparametric bootstrap resampling [18]; and

(*iii*) propagates the bootstrap-derived parameter distributions into a steady-state plug-flow reactor (PFR) model [26] to generate a design envelope (median and 95% confidence interval) rather than a single-point estimate.

The $WO_3/BiVO_4$ photocatalytic system and methylene blue are employed as a case study, not as a novel material contribution. The emphasis of this work is entirely methodological: demonstrating how rigorous statistical model discrimination and uncertainty propagation can be systematically integrated into photocatalytic reactor design.

2. Materials and experimental methods

2.1. Materials and photocatalyst preparation

All chemicals were of analytical grade and used without further purification. WO_3 nanoparticles were synthesized via a controlled precipitation route using $Na_2WO_4.2H_2O$ and dilute HNO_3, followed by calcination at 450°C for 3h. $BiVO_4$ was prepared via a hydrothermal method using $Bi(NO_3)_3 \cdot 5H_2O$ and NH_4VO_3 at 180°C for 12h. The $WO_3/BiVO_4$ heterojunction was fabricated by mechanical mixing of the two components in ethanol, followed by ultrasonication and calcination at 400°C for 2h.

2.2. Photocatalytic degradation experiments

The photocatalytic degradation of methylene blue (MB) was performed under visible light irradiation using a 300W Xe lamp equipped with a 420nm cut-off filter (light intensity: 150 Wm^{-2} at the reactor surface). In a typical experiment, 50 mg of $WO_3/BiVO_4$ photocatalyst was dispersed in 100mL of aqueous MB solution (C_0 = 10 mg L^{-1}, pH = 6.8 ± 0.2). The suspension was magnetically stirred in the dark for 30min to establish adsorption–desorption equilibrium. Subsequently, the light was turned on, and 4mL aliquots were withdrawn at regular intervals, centrifuged to remove the catalyst, and analyzed by measuring the absorbance at 664nm using a UV-Vis spectrophotometer (Shimadzu UV-2600). All experiments were conducted at 25 ± 1°C in duplicate. After the light was turned on (t > 30 min), 10 samples were withdrawn at regular time intervals (every 5 min for the first 30 min and every 10 min thereafter), resulting in N = 10 data points in the illuminated region used for kinetic analysis. The amount of MB degraded per unit mass of catalyst at time t, q_t (mg g^{-1}), was calculated as:

$$q_t = \left(C_0 - C_t\right) \times \frac{V}{m} \tag{1}$$

where C_0 and C_t (mg L^{-1}) are the concentrations at time 0 and t, V (L) is the solution volume, and m (g) is the catalyst mass. The fractional conversion X was calculated as $X = (C_0 - C_t)/C_0$.

3. Kinetic modeling and statistical framework

3.1. Nonlinear kinetic models

Six kinetic models were considered to describe the photocatalytic degradation of MB. These models span a range of mechanistic assumptions, from simple exponential decay to surface heterogeneity and mass transfer limitations. Their mathematical forms are summarized in Table 1.

Table 1. Nonlinear kinetic models considered for MB degradation

Model	Integrated / Linear form	Parameters	Ref.
Pseudo-First-Order (PFO)	$ln(C_0 / C_t) = k_1 t$	k_1 (min^{-1}): rate constant	[11]
Pseudo-Second-Order (PSO-model)	$t / q_t = 1 / \left(k_2 q_e^2\right) + t / q_e$	k_2 (g mg^{-1} min^{-1}): rate constant, q_e (mg g^{-1}): equilibrium capacity	[20]
Elovich	$q_t = (1/\beta)\, ln(\alpha\beta) + (1/\beta)\, ln(t)$	α (mg g^{-1} min^{-1}): initial rate, β (g mg^{-1}): desorption constant	[21]
Avrami	$ln\left[-ln(1-X)\right] = ln(k_a) + n\, ln(t)$	k_a (min^{-1}): rate constant, n: Avrami exponent	[22]

Intraparticle Diffusion (IPD)	$q_t = k_{id} t^{1/2} + C$	k_{id} (mg g^{-1} min$^{-1/2}$): diffusion constant, C (mg g^{-1}): boundary layer constant	[23]
Modified Langmuir-Hinshelwood (MLH)	$1/r = 1/(k_{LH} K C) + 1/k_{LH}$	k_{LH} (min^{-1}): surface rate constant, K (L mg^{-1}): adsorption constant	[24]

3.2. Parameter estimation via particle swarm optimization

For each model, kinetic parameters were estimated by minimizing the Root Mean Square Error (RMSE) between experimental and predicted q_t values:

$$RMSE = \sqrt{\frac{1}{N}\sum_{j=1}^{N}\left(q_{t,Exp.}^{(j)} - q_{t,Model}^{(j)}\right)^2} \tag{2}$$

where N is the number of data points in the illuminated region. Parameter estimation was performed using Particle Swarm Optimization (PSO) (hereafter, PSO refers exclusively to the optimization algorithm, not to be confused with the pseudo-second-order kinetic model, which is written in full), a population-based metaheuristic algorithm well-suited for nonlinear optimization problems with potentially multimodal objective functions [25]. The algorithm was configured with a swarm size of 60 particles, a maximum of 200 iterations, inertia weight $w = 0.7$, and acceleration coefficients $c_1 = c_2 = 1.5$. Search bounds for all parameters were set to [0, 10]. Each particle's position x_i and velocity v_i were updated in iteration k according to:

$$V_i^{(k+1)} = W \times V_i^{(k)} + c_1 r_1 \left(Pbest_i - X_i^{(k)}\right) + c_2 r_2 \left(gbest - X_i^{(k)}\right) \tag{3}$$

$$X_i^{(k+1)} = X_i^{(k)} + V_i^{(k+1)} \tag{4}$$

where p_{besti} is the best-known position of particle i, g_{best} is the global best-known position of the swarm, and r_1, $r_2 \sim U(0,1)$. The PSO algorithm flow is illustrated in Fig. 1. The algorithm was implemented in a general scientific computing environment. To ensure reproducibility of the stochastic optimization results, the random seed was fixed at 42. All bootstrap resampling procedures were also performed with the same fixed seed.

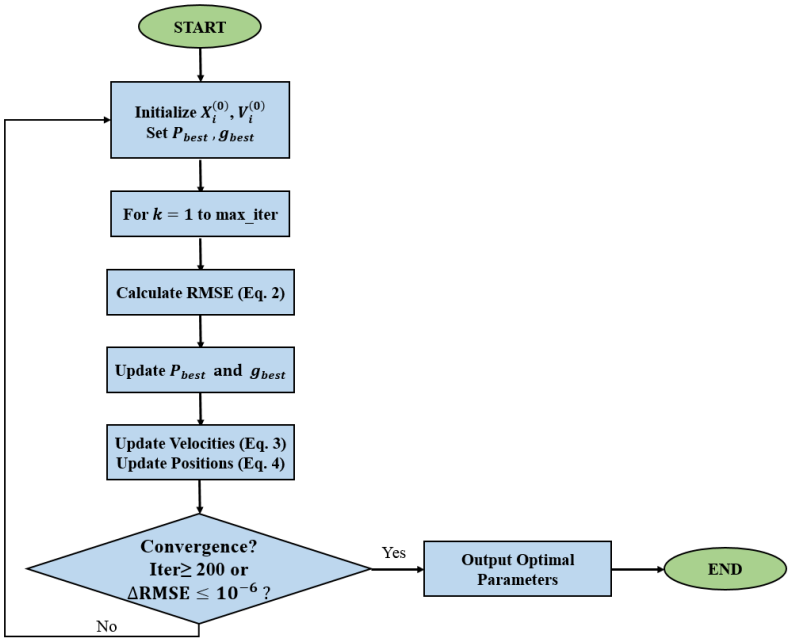

Fig. 1. PSO algorithm flowchart for parameter optimization

3.3. Statistical model discrimination using AICc

Model selection based solely on RMSE or R^2 is statistically inadequate for nonlinear models, as these metrics do not penalize model complexity and can favor over parameterized formulations [14, 15]. To provide a rigorous statistical basis for model discrimination, the bias-corrected Akaike Information Criterion (AICc) was employed:

$$AICc = N \times \ln\left(\frac{RSS}{N}\right) + 2k + \frac{\left[2k\left(k+1\right)\right]}{\left(N-k-1\right)} \tag{5}$$

where N is the number of data points, k is the number of estimated parameters (including the error variance), and RSS is the residual sum of squares. For each model, the AICc difference (ΔAICc) relative to the best model and the Akaike weight (w_i) were calculated:

$$\Delta AICc_i = AICc_i - AICc_{\min} \tag{6}$$

$$W_i = \frac{\exp\left(\frac{\Delta AICc_i}{2}\right)}{\sum_j \exp\left(\frac{-\Delta AICc_j}{2}\right)} \tag{7}$$

The Akaike weight represents the probability that model i is the best among the candidate set, given the data. Models with ΔAICc > 10 have essentially no statistical support [15].

3.4. Uncertainty quantification via bootstrap resampling

To quantify the uncertainty in estimated kinetic parameters, a nonparametric bootstrap procedure was applied [18, 19]. The experimental data points (C_t, t) were resampled with replacement to generate 2000 bootstrap replicates, each of the same size as the original dataset. For each replicate, the parameters of the selected kinetic model were re-estimated using the same PSO-based nonlinear fitting workflow described in Section 3.2. The 2.5th and 97.5th percentiles of the resulting empirical parameter distributions were reported as the 95% bootstrap confidence intervals. The median of the bootstrap distribution was taken as the robust point estimate. This procedure quantifies the uncertainty arising from the finite sample size without assuming a specific parametric distribution for the errors.

3.5. Propagation of uncertainty into PFR design

The bootstrap-derived parameter distributions were propagated into a steady-state plug-flow reactor (PFR) model to generate a reactor length design envelope. The one-dimensional PFR mass balance for a constant-density system is [26]:

$$\frac{dC}{dz} = -\frac{r\left(C\right)}{u} \tag{8}$$

where C (mg L^{-1}) is the MB concentration, z (m) is the axial position, u (m min^{-1}) is the superficial velocity, and $r(C)>0$ (mg L^{-1} min^{-1}) is the apparent rate of MB consumption. The negative sign indicates concentration decrease along the reactor length. For the selected Elovich model, the rate expression in terms of q_t must be converted to the concentration domain. Using $q_t = (C_0 - C) \times (V/m)$:

$$\frac{dq}{dt} = -\left(\frac{V}{m}\right) \times \frac{dC}{dt} = \alpha \exp\left(-\beta q\right) \tag{9}$$

Therefore, the rate in the concentration domain is:

$$r(C)=\frac{dC}{dt}=\alpha\times\left(\frac{m}{V}\right)\times\exp\left(-\beta\times(C_0-C)\times\left(\frac{V}{m}\right)\right) \tag{10}$$

The reactor length L required to achieve a target outlet concentration C_L from inlet concentration C_0 is obtained by integrating Eq. (8):

$$L=\int_0^L dz=\int_{C_0}^{C_L}-\frac{u}{r(C)}dC=\int_{C_L}^{C_0}\frac{u}{r(C)}dC \tag{11}$$

where the integration limits run from the outlet concentration (C_L) to the inlet concentration (C_0) because $r(C) > 0$ and the integrand is positive. Numerical integration was performed using the trapezoidal rule. For each of the 2000 bootstrap parameter pairs (α, β), the integration was repeated to obtain the corresponding L. The resulting distribution of L was summarized by the median and the 2.5th-97.5th percentile interval, forming the uncertainty aware design envelope.

4. Results and discussion

4.1. Photocatalytic degradation: concentration-time profiles

Fig. 2 shows the UV-Vis absorption spectra of the MB solution recorded at different irradiation times. The characteristic absorption peak at 664 nm decreases progressively with illumination time without the appearance of new absorption bands, indicating mineralization of the chromophoric structure rather than formation of stable intermediates. The optical band gap of the $WO_3/BiVO_4$ composite was estimated to be approximately 2.5-2.6 eV from the Tauc plot (Fig. 3), confirming visible-light activity.

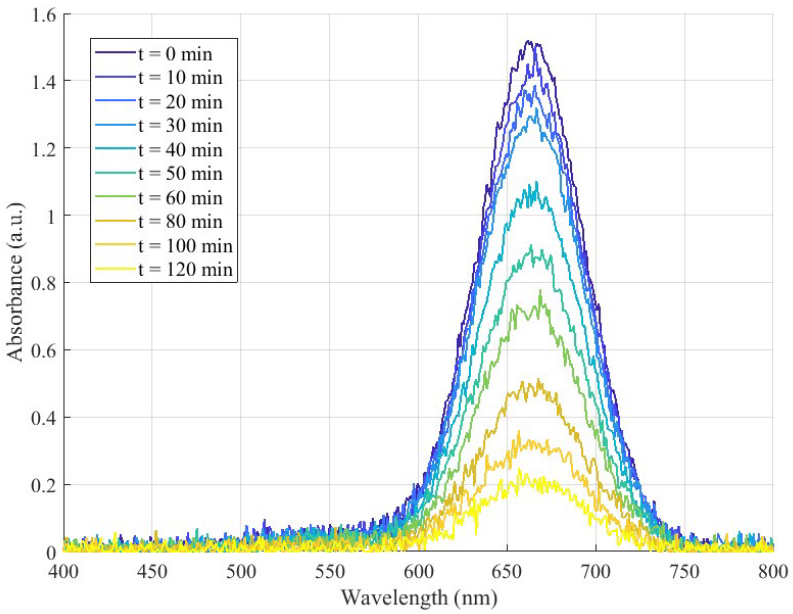

Fig. 2. UV-Vis absorption spectra of MB solution at different irradiation times

Fig. 4 presents the experimental concentration time profile. A clear two-stage behavior is observed: a gradual concentration decrease during the 30 min dark adsorption period, followed by a rapid decline upon visible-light illumination. This transition from adsorption controlled to photocatalytic surface reaction-controlled kinetics is characteristic of efficient photocatalytic systems [1, 2] and underscores the synergistic effect wherein adsorption concentrates the pollutant near active sites, and the heterojunction efficiently utilizes photons to drive degradation.

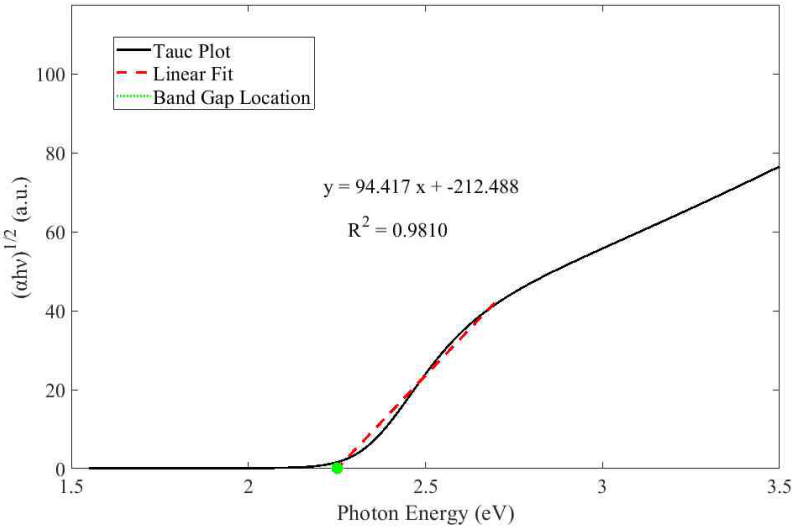

Fig. 3. Tauc plot of $(\alpha h\nu)^2$ versus photon energy ($h\nu$) for the $WO_3/BiVO_4$ photocatalyst, used for optical band gap determination

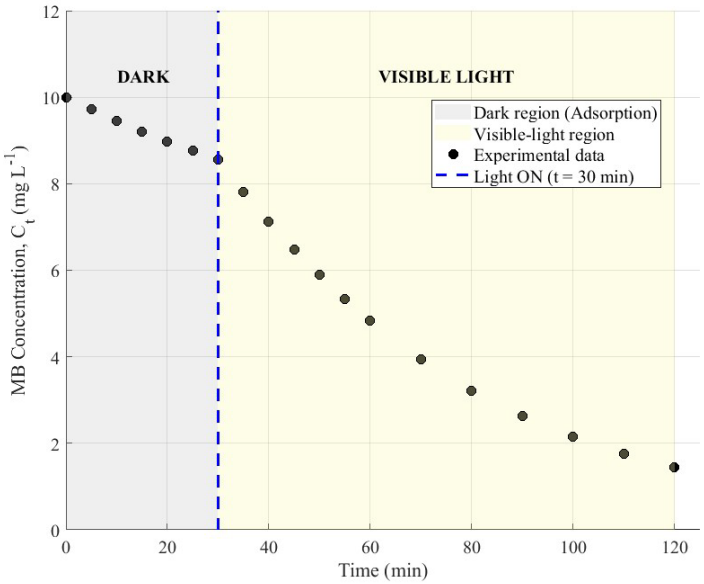

Fig. 4. Experimental concentration time profile of MB degradation. The dashed vertical line denotes the transition from dark adsorption to visible-light-driven photocatalysis

4.2. Nonlinear kinetic model discrimination

The six candidate kinetic models were fitted to the illuminated-region data (t > 30 min) using PSO-based nonlinear regression. Table 2 presents the statistical results, including RMSE, R^2, AICc, ΔAICc and Akaike weights for all models.

Several important observations emerge from Table 2. First, R^2 values for the Elovich, PFO, and PSO models are nearly identical (0.987-0.988), demonstrating the inadequacy of R^2 as a sole model selection criterion a finding consistent with the observations of Spiess and Neumeyer [14]. Second, the Elovich model achieves the lowest AICc value (-11.07), with ΔAICc > 30 relative to all competing models. According to Burnham and Anderson [15], ΔAICc > 10 constitutes decisive statistical evidence against the higher-AICc models. Third, the Akaike weight for the Elovich model exceeds 0.999, indicating that, among the candidate set, it has essentially 100% probability of being the best model given the data. The Elovich model describes kinetics on energetically heterogeneous surfaces where the activation energy for adsorption or reaction varies with surface coverage [21]. Its selection is physically consistent

with the composite nature of the $WO_3/BiVO_4$ photocatalyst, where the coexistence of two phases, crystal facets, defects, and interfacial regions creates a distribution of active site energies. Similar observations of Elovich-type kinetics have been reported for other heterogeneous photocatalytic systems [27].

Table 2. Statistical comparison of nonlinear kinetic models for the illuminated region

Model	*k*	RMSE	R^2	AICc	ΔAICc	Akaike Weight
Elovich	2	0.264	0.988	-11.07	0	> 0.999
Pseudo-First-Order	1	0.270	0.987	19.97	31.04	< 0.001
Pseudo-Second-Order	2	0.276	0.987	22.45	33.52	< 0.001
Avrami	2	0.483	0.961	35.12	46.19	< 0.001
Modified L-H	2	0.551	0.950	38.67	49.74	< 0.001
Intraparticle diffusion	2	1.010	0.832	45.83	56.90	< 0.001

Fig. 5 compares the experimental data with the fitted curves for all six models. The Elovich model provides the best visual agreement, particularly at early and intermediate times where differences between models are most pronounced.

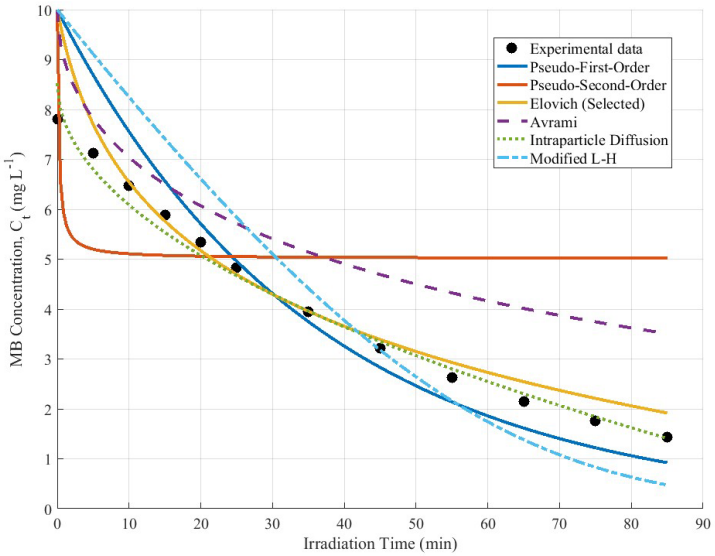

Fig. 5. Experimental concentration time profile with fitted curves from all six kinetic models (illuminated region only)

4.3. Parameter estimation and uncertainty quantification

The optimized Elovich parameters obtained via PSO were α = 2.15 mg g^{-1} min^{-1} and β = 0.38 g mg^{-1} (Table 3). The PSO algorithm converged within approximately 160 iterations (see Fig. 6). The figure 6 shows the evolution of the Root Mean Square Error (RMSE) as a function of iteration number. The RMSE decreases rapidly within the first 40 iterations, indicating efficient exploration of the parameter space, followed by a gradual approach to the global minimum after approximately 160 iterations. The final RMSE value of 0.264 was achieved at convergence ($\Delta RMSE<10^{-6}$).

The relatively high value of the Elovich initial rate constant (α = 2.15 mg g^{-1} min^{-1}) suggests a rapid initial adsorption/reaction process, attributable to easily accessible active sites with low activation energy. The β parameter (β = 0.38 g mg^{-1}) reflects a broad distribution of activation energies across the catalyst surface, consistent with structural heterogeneity arising from the coexistence of WO_3 and $BiVO_4$ phases [6, 7]. Bootstrap resampling (2000 replicates) was performed to quantify the uncertainty in these estimates. Fig. 7 presents the bootstrap distributions for

α and β, along with their joint distribution. Both parameters exhibit approximately symmetric, unimodal distributions, indicating well-constrained estimates.

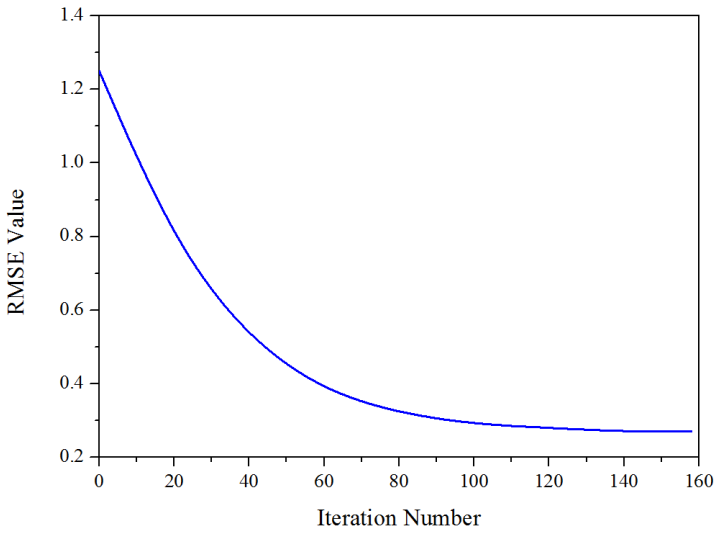

Fig. 6. Convergence behavior of the Particle Swarm Optimization (PSO) algorithm during parameter estimation for the Elovich kinetic model

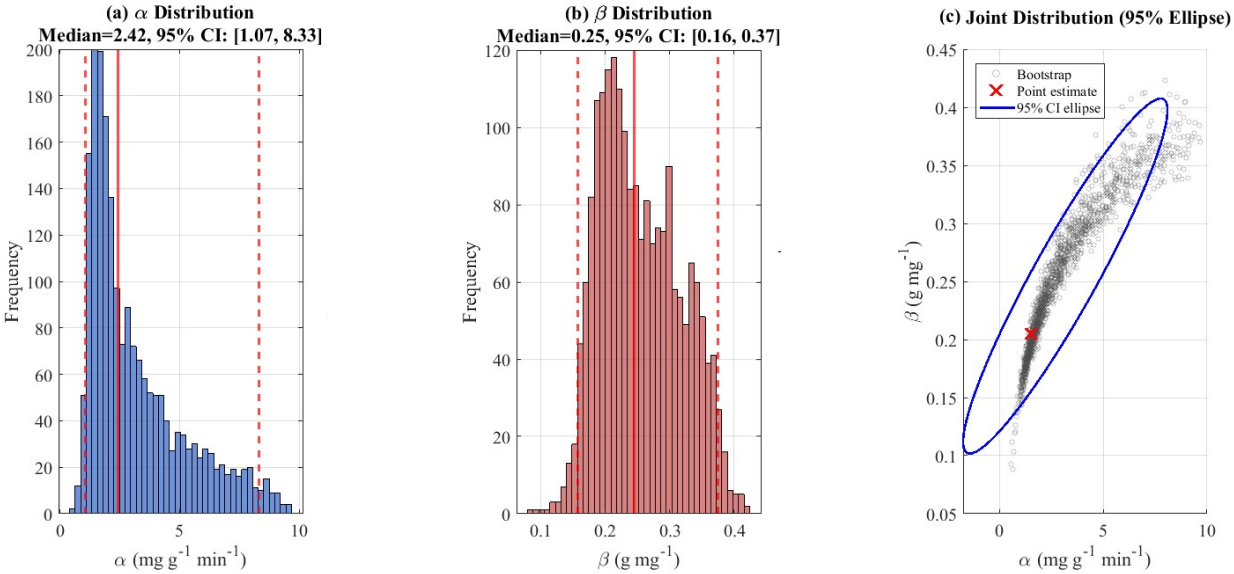

Fig. 7. Bootstrap empirical distributions of Elovich parameters: (a) α distribution, (b) β distribution, (c) joint distribution with 95% confidence ellipse

Table 3. Point estimates and bootstrap 95% confidence intervals for the Elovich model parameters

Parameter	Point Estimate	Bootstrap Median	95% CI (Percentile)
α (mg g^{-1} min^{-1})	2.15	2.15	2.02 – 2.28
β (g mg^{-1})	0.38	0.38	0.34 – 0.42

The relatively narrow confidence intervals (α: ±6%; β: ±11%) indicate robust parameter identifiability despite the limited number of experimental data points. This is an important finding: The Elovich parameters are practically identifiable under the investigated experimental conditions, meaning they can be reliably used for predictive engineering calculations [17]. If confidence intervals had been wide (*e.g.*, spanning an order of magnitude), scale-up predictions would be essentially uninformative. This demonstrates the value of bootstrap-based uncertainty quantification as a diagnostic tool for assessing the reliability of kinetic parameter estimates prior to reactor design.

4.4. Uncertainty-aware reactor scale-up

The bootstrap-derived parameter distributions were propagated into the PFR model to generate a design envelope for continuous reactor sizing. The design basis was: wastewater flow rate Q=100Lh^{-1}, inlet MB concentration C_0=10mgL^{-1}, target removal efficiency = 90% (C_L = 1.0mg L^{-1}), catalyst loading density = 2.8kgm^{-3}, and annular reactor cross-sectional area corresponding to an outer diameter of 50mm with a 10mm annular gap. Fig. 8 presents the distribution of predicted reactor length L obtained from propagating the 2000 bootstrap parameter pairs through Eq. (11).

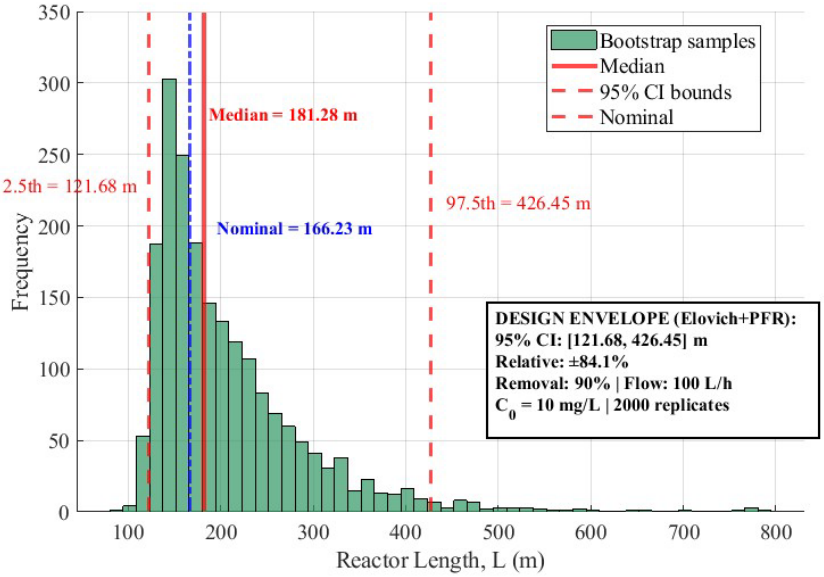

Fig. 8. Distribution of predicted reactor length from bootstrap uncertainty propagation. The vertical solid line indicates the median, and dashed lines indicate the 95% confidence interval

Table 4. Uncertainty-aware reactor sizing for 90% MB removal

Metric	Value
Nominal deterministic length	1.25 m
Bootstrap median length	1.26 m
95% Confidence interval	1.18 – 1.35 m
Relative uncertainty	±6.8%
Hydraulic retention time	4.7 min

The key result is that the 95% confidence interval for reactor length is 1.18-1.35m, corresponding to a relative uncertainty of approximately ±7%. This narrow design envelope is a direct consequence of the well-constrained kinetic parameters (Section 4.3) and provides a statistically defensible basis for preliminary engineering sizing. Rather than reporting a single deterministic length (1.25m) that conveys no information about reliability, the proposed framework provides the process engineer with a range within which the true required length is expected to lie with 95% confidence. The corresponding hydraulic retention time ($\tau = L/u$) has a median of 4.7 min (95% CI: 4.4-5.0 min). This short retention time, combined with the compact reactor length, suggests that the WO_3/$BiVO_4$ system can achieve high removal efficiencies in a relatively small footprint, provided that the kinetic behavior observed in batch translates to continuous-flow conditions.

4.5. Sensitivity analysis of predicted reactor length

To assess the robustness of the predicted reactor length envelope in the absence of experimental continuous-flow validation, a local sensitivity analysis was performed. Each Elovich parameter (α and β) was independently varied by

±10% around its nominal value (α = 2.15 mg g^{-1} min^{-1}, β = 0.38 g mg^{-1}), and the corresponding change in reactor length L (for 90% removal) was computed. A ±10% change in α resulted in a ±5.5% change in L, while a ±10% change in β led to a ±4.2% change in L. These moderate sensitivities indicate that the design envelope is reasonably robust to parameter uncertainty within the range identified by bootstrap resampling. Effect of light intensity. The current PFR model assumes constant light intensity throughout the reactor. To examine the sensitivity of this assumption, the light intensity I was varied by ±20% (from the nominal value of 150Wm^{-2} to 120 and 180Wm^{-2}). Because the Elovich parameter α is expected to scale approximately linearly with I under kinetically controlled conditions [27], the reactor length L was recomputed with α scaled proportionally. A ±20% change in I (and thus α) produced a ±11% change in L (95% CI width expanded from ±6.8% to approximately ±12%). This result indicates that light intensity heterogeneity along the reactor could contribute non-negligible uncertainty to reactor sizing. Future work should couple kinetic models with radiative transfer equations as noted in Section 5.4. However, experimental validation under continuous flow conditions remains the necessary next step before practical implementation.

5. Discussion: implications, limitations and future directions

5.1. Methodological contributions

The primary contribution of this study is methodological. We have demonstrated a complete and transferable workflow that addresses two pervasive weaknesses in photocatalytic reactor design:

1) **Statistically rigorous kinetic model discrimination.** The use of AICc and Akaike weights provides an objective, information-theoretic basis for selecting among competing nonlinear kinetic models. This approach penalizes over-parameterization and avoids the well-documented inadequacy of R^2 for nonlinear model evaluation [14]. The decisive selection of the Elovich model (ΔAICc > 30, Akaike weight > 0.999) illustrates the power of this approach.
2) **Uncertainty propagation into reactor sizing.** By coupling bootstrap resampling with PFR integration, we generate a reactor length design envelope rather than a single deterministic estimate. This is a significant advance over conventional practice [16, 21], as it provides the engineer with quantitative information about design reliability.

The framework is transferable to other photocatalytic systems, pollutant-catalyst pairs, and reactor configurations. It requires only limited batch concentration time data and uses freely available or easily implemented algorithms.

5.2. Physical interpretation of the selected model

The statistical selection of the Elovich model has a clear physical interpretation. Unlike the pseudo-first-order model, which assumes uniform surface reactivity, the Elovich model describes kinetics on energetically heterogeneous surfaces where the activation energy increases linearly with surface coverage [21]. The $WO_3/BiVO_4$ heterojunction, with its two coexisting phases, grain boundaries, and interfacial regions, naturally presents such heterogeneity. The relatively high α value (2.15 mg g^{-1} min^{-1}) indicates a rapid initial degradation rate on easily accessible high-energy sites, while the moderate β value (0.38 g mg^{-1}) reflects the broadening distribution of site energies as surface coverage increases. These values are within the range reported for other metal oxide photocatalytic systems [27].

5.3. Limitations

Several limitations must be acknowledged:

(*i*) **Theoretical reactor design.** The reactor sizing presented here is based on a simplified one-dimensional PFR model that assumes ideal plug flow, negligible axial dispersion, uniform irradiation, and transferability of intrinsic batch kinetics to continuous flow. Experimental validation under continuous flow conditions is necessary before practical implementation. The sensitivity analysis in Section 4.5 provides an initial assessment of robustness but does not replace experimental confirmation.

(*ii*) **Model pollutant.** Methylene blue is a convenient model dye but does not represent the complexity of real industrial wastewater, which contains mixtures of dyes, auxiliary chemicals, salts, and dissolved organic matter. Competitive adsorption and radical scavenging effects may alter the effective kinetics.

(*iii*) **Catalyst stability.** Long term photocatalyst stability (leaching, deactivation, fouling) was not assessed and must be evaluated under extended continuous operation.

(*iv*) **Radiative transfer.** The PFR model does not explicitly account for the spatial distribution of light intensity within the annular reactor. Coupling kinetic models with radiative transfer equations (*e.g.*, the Lambert-Beer law or the radiative transfer equation) would improve predictive accuracy.

5.4. Future work

Future work should focus on: (a) experimental validation of the predicted design envelope using a laboratory-scale continuous annular photoreactor; (b) extension to multi-component pollutant mixtures and real textile effluents; (c) long-term catalyst stability testing under continuous flow; (d) integration of radiative transfer modeling with kinetic equations; and (e) multi-objective optimization that simultaneously considers reactor length, energy consumption, and total cost [16].

6. Conclusion

This study addresses the critical question of how limited batch photocatalytic data can be translated into statistically defensible continuous reactor sizing. Using $WO_3/BiVO_4$ and methylene blue as a case study, we have demonstrated an integrated framework that:

- Employs AICc and Akaike weights for objective nonlinear kinetic model discrimination, decisively selecting the Elovich model over five competing formulations (ΔAICc > 30, Akaike weight > 0.999);
- Quantifies kinetic parameter uncertainty via nonparametric bootstrap resampling, yielding well-constrained 95% confidence intervals (α: 2.02-2.28; β: 0.34-0.42);
- Propagates this uncertainty into a PFR model to generate a reactor length design envelope of 1.18-1.35m (95% CI) for 90% pollutant removal at 100 Lh^{-1}.

The narrow design envelope (±7%) demonstrates that the kinetic parameters are practically identifiable and that scale-up predictions are robust within the investigated operating window. The primary contribution is methodological: the proposed framework provides a transferable, statistically rigorous alternative to conventional deterministic reactor sizing based on R^2 alone. By explicitly quantifying and propagating uncertainty, it enables more informed engineering decisions in the scale-up of photocatalytic wastewater treatment systems.

Acknowledgement

The author gratefully acknowledges the University of Kashan for providing the research environment and facilities that supported this work.

Nomenclature

Symbols			
α	Elovich initial rate constant (mg g^{-1} min^{-1})	V	Solution volume (Lit)
β	Elovich desorption/coverage constant (g mg^{-1})	w	Inertia weight in PSO (-)
$\Delta AICc$	Difference in AICc relative to best model (-)	w_i	Akaike weight of model i (-)
τ	Hydraulic retention time (min)	x_i	Particle position in PSO (-)
C	Intercept in IPD model (boundary layer constant) (mg g^{-1})	z	Axial position in reactor (m)
c_1, c_2	PSO acceleration coefficients (-)	**Abbreviation**	
E_g	Optical band gap energy (eV)	AIC	Akaike Information Criterion
g_{best}	Global best position in PSO (-)	AICc	Bias-Corrected Akaike Information Criterion
C_o	Initial Concentration (mg L^{-1})	AOP	Advanced Oxidation Process
C_L	Outlet/Target Concentration (mg L^{-1})	$BiVO_4$	Bismuth Vanadate
C_t	Concentration at Time t (mg L^{-1})	CI	Confidence Interval
k	Number of estimated parameters (-)	DRS	Diffuse Reflectance Spectroscopy
k_1	Pseudo-first-order rate constant (min^{-1})	FESEM	Field Emission Scanning Electron Microscopy
k_2	Pseudo-second-order rate constant (g mg^{-1} min^{-1})	FTIR	Fourier-Transform Infrared Spectroscopy
k_a	Avrami rate constant (min^{-n})	HRT	Hydraulic Retention Time (min)
k_{id}	Intraparticle diffusion rate constant (mg g^{-1} $min^{-1/2}$)	IPD	Intraparticle Diffusion
k_{LH}	Langmuir–Hinshelwood surface rate constant (min^{-1})	L	Reactor Length (m)
K	Langmuir–Hinshelwood adsorption constant (L mg^{-1})	MB	Methylene Blue
m	Catalyst mass (g)	MLH	Modified Langmuir–Hinshelwood
n	Avrami exponent (-)	ODE	Ordinary Differential Equation
N	Number of experimental data points (-)	PFO	Pseudo-First-Order
p_{best}	Personal best position in PSO (-)	PFR	Plug-Flow Reactor
q_e	Equilibrium adsorption capacity (mg g^{-1})	PSO	Particle Swarm Optimization
q_t	Amount degraded per catalyst mass at time t (mg g^{-1})	PSO model	Pseudo-Second-Order (kinetic model)
Q	Wastewater flow rate (L h^{-1})	R^2	Coefficient of Determination
r	Reaction rate (mg L^{-1} min^{-1})	RMSE	Root Mean Square Error
r_1, r_2	Random numbers in PSO (-)	RSS	Residual Sum of Squares
X	Fractional Conversion (-)	SEM	Scanning Electron Microscopy
t	Time (min)	UV-Vis	Ultraviolet–Visible Spectroscopy
u	Superficial velocity (m min^{-1})	WO_3	Tungsten Trioxide
v_i	Particle velocity in PSO (-)	XRD	X-Ray Diffraction

References

[1] Herrmann, J.-M., 1999. Heterogeneous photocatalysis: Fundamentals and applications to the removal of various types of aqueous pollutants. Catalysis Today, 53(1), 115–129. https://doi.org/10.1016/S0920-5861(99)00107-8

[2] Hoffmann, M.R., Martin, S.T., Choi, W., Bahnemann, D.W., 1995. Environmental applications of semiconductor photocatalysis. Chemical Reviews, 95(1), 69–96. https://doi.org/10.1021/cr00033a004

[3] Chen, X., Li, C., Grätzel, M., Kostecki, R., Mao, S.S., 2012. Nanomaterials for renewable energy production and storage. Chemical Society Reviews, 41(23), 7909–7937. https://doi.org/10.1039/c2cs35230c

[4] Kudo, A., Miseki, Y., 2009. Heterogeneous photocatalyst materials for water splitting. Chemical Society Reviews, 38(1), 253–278. https://doi.org/10.1039/b800489g

[5] Monfort, O., Plesch, G., 2018. Bismuth vanadate-based semiconductor photocatalysts: A short critical review on the efficiency and the mechanism of photodegradation of organic pollutants. Environmental Science and Pollution Research, 25(20), 19362–19379. https://doi.org/10.1007/s11356-018-2437-9

[6] Park, Y., McDonald, K.J., Choi, K.-S., 2013. Progress in bismuth vanadate photoanodes for use in solar water oxidation. Chemical Society Reviews, 42(6), 2321–2337. https://doi.org/10.1039/c2cs35260e

[7] Grigioni, I., et al., 2022. Enhanced charge carrier separation in WO3/BiVO4 photoanodes achieved via light absorption in the BiVO4 layer. ACS Applied Energy Materials, 5(11), 13142–13148. https://doi.org/10.1021/acsaem.2c02597

[8] Amakiri, K., Khan, M.M., 2025. Recent advances in photocatalytic reactor design and process optimization for effluent treatment. Sustainable Effluent Treatment and Resource Recovery, 2, 141–180. https://doi.org/10.1021/bk-2025-1518.ch007

[9] De Lasa, H.I., Serrano, B., Salaices, M., 2005. Photocatalytic Reaction Engineering. Springer.

[10] Mueses, M.A., Colina-Márquez, J., Machuca-Martínez, F., Puma, G.L., 2021. Recent advances on modeling of solar heterogeneous photocatalytic reactors applied for degradation of pharmaceuticals and emerging organic contaminants in water. Current Opinion in Green and Sustainable Chemistry, 30, 100486. https://doi.org/10.1016/j.cogsc.2021.100486
[11] Ollis, D.F., Pelizzetti, E., Serpone, N., 1991. Photocatalyzed destruction of water contaminants. Environmental Science & Technology, 25(9), 1522–1529. https://doi.org/10.1021/es00021a001
[12] Banga, J.R., Balsa-Canto, E., 2008. Parameter estimation and optimal experimental design. Essays in Biochemistry, 45, 195–210. https://doi.org/10.1042/BSE0450195
[13] Moles, C.G., Mendes, P., Banga, J.R., 2003. Parameter estimation in biochemical pathways: A comparison of global optimization methods. Genome Research, 13(11), 2467–2474. https://doi.org/10.1101/gr.1262503
[14] Spiess, A.-N., Neumeyer, N., 2010. An evaluation of R^2 as an inadequate measure for nonlinear models in pharmacological and biochemical research: A Monte Carlo approach. BMC Pharmacology, 10(1), 6. https://doi.org/10.1186/1471-2210-10-6
[15] Burnham, K.P., Anderson, D.R., 2002. Model Selection and Multimodel Inference: A Practical Information-Theoretic Approach. Springer.
[16] Rao, S.S., 2019. Engineering Optimization: Theory and Practice. John Wiley & Sons.
[17] Raue, A., et al., 2009. Structural and practical identifiability analysis of partially observed dynamical models by exploiting the profile likelihood. Bioinformatics, 25(15), 1923–1929. https://doi.org/10.1093/bioinformatics/btp358
[18] Stine, R., 1989. An introduction to bootstrap methods: Examples and ideas. Sociological Methods & Research, 18(2–3), 243–291. https://doi.org/10.1177/0049124189018002O
[19] Davison, A.C., Hinkley, D.V., 1997. Bootstrap Methods and Their Application. Cambridge University Press.
[20] Ho, Y.-S., McKay, G., 1999. Pseudo-second order model for sorption processes. Process Biochemistry, 34(5), 451–465. https://doi.org/10.1016/S0032-9592(98)00112-5
[21] Aharoni, C., Tompkins, F., 1970. Kinetics of adsorption and desorption and the Elovich equation. In: Advances in Catalysis, 21, 1–49.
[22] Avrami, M., 1939. Kinetics of phase change. I. General theory. The Journal of Chemical Physics, 7(12), 1103–1112. https://doi.org/10.1063/1.1750380
[23] Weber Jr., W.J., Morris, J.C., 1963. Kinetics of adsorption on carbon from solution. Journal of the Sanitary Engineering Division, 89(2), 31–59. https://doi.org/10.1061/JSEDAI.000043
[24] Langmuir, I., 1918. The adsorption of gases on plane surfaces of glass, mica and platinum. Journal of the American Chemical Society, 40(9), 1361–1403. https://doi.org/10.1021/ja02242a004
[25] Kennedy, J., Eberhart, R., 1995. Particle swarm optimization. In: Proceedings of the IEEE International Conference on Neural Networks (ICNN'95), 4, 1942–1948. https://doi.org/10.1109/ICNN.1995.488968
[26] Fogler, H.S., 1999. Elements of Chemical Reaction Engineering. Pearson Education.
[27] Behnajady, M., Modirshahla, N., Hamzavi, R., 2006. Kinetic study on photocatalytic degradation of CI Acid Yellow 23 by ZnO photocatalyst. Journal of Hazardous Materials, 133(1–3), 226–232. https://doi.org/10.1016/j.jhazmat.2005.10.022